



Towards maximizing the sensing accuracy of an cuffless, optical blood pressure sensor using a high-order front-end filter

Yung-Hua Kao¹ · Paul C.-P. Chao¹ · Chin-Long Wey¹

Received: 17 November 2017 / Accepted: 30 March 2018 / Published online: 6 April 2018
© Springer-Verlag GmbH Germany, part of Springer Nature 2018

Abstract

A high-order filter as part of an analog front-end circuit for an optical, cuffless photoplethysmography (PPG) sensor is developed herein to maximize the sensing accuracy of measured blood pressures (BPs). The BP device consists physically of light emitting diodes and photo-diodes (PDs) to sense the dynamic change of intravascular blood volume based on the known principle of PPG and then calculate the BP based on reflective pulse transient time in a PPG signal. The photoplethysmography (PPG) signal acquired by the PDs are expected to be processed by an excellent front-end circuitry to reduce its noise and DC offset but without much distortion to obtain accurate BP prediction. This front-end is accomplished herein by a transimpedance amplifier, a critical high-order band-pass filter and a programmable gain amplifier, which is followed by microprocessor and a wireless module. The band-pass filter is optimized with a passband from 0.2 to 7.2 Hz, where the low-pass is in a 4th order while the high-pass is in 2nd order. The low-pass is designed for reducing noise including those due to ambient lighting, while the high-pass is for reducing DC drifting caused mainly by breathing and/or subject slow motion. 46 subjects were tested with the designed high-order filters in comparison with reference device. The advantages of employing high-order low-pass filter versus first-order is clearly seen in experimental data with an accuracy on predicting BP reaching ± 3 mmHg, as stopped to ± 7 mmHg using commonly used first-order filters.

1 Introduction

According to WHO reports, approximate 17.5 million people suffer cardiovascular diseases (CVDs) in 2015 (WHO, World health statistic 2015, 2015b). The number is estimated to reach 23.3 million by 2030 (WHO, Cardiovascular diseases, 2015a). The people with CVDs died each year an estimated 31% of all deaths worldwide. The arterial blood pressure (BP) is highly correlated to cardiovascular system. This is why the BP measurement is an important indicator of cardiovascular diseases (Ahmad et al. 2010a, b; Dupuis and Eugene 2000; Silvani et al. 2008).

Towards the continuous BP measurement with minimum discomfort, much recent effort was devoted to develop cuffless BP sensors (Sharma et al. 2017, Lin et al. 2017). To date, there are two different types of cuffless BP sensors are under intensive effort of development. They are contact-type skin vibration sensors and photoplethysmography (PPG) sensors.

Kaniusas et al. (2006) proposed a cuffless magnetoelastic skin curvature sensor to achieve continuous BP measurement with assistance of an ECG sensor (Lee and Cheng 2009, Mahmoud et al. 2014, Huang et al. 2015). Using this sensor, the skin vibration due to arterial pulsation at wrist is continuously measured to estimate DBPs and SBPs. Chao (Tu et al. 2013, 2014; Kao et al. 2016) designed another type of curvature sensor which embeds metal electrodes, the piezo-resistance of which varies with skin vibration. Despite the merit of cufflessness, the accuracy of these newly-proposed skin vibration sensors is highly sensitive to placement imprecision of the sensor off the sweat wrist spot where there is maximum pulsation. As for the PPG sensors, which mainly consist of light emitting diode (LED), photodiode (PD) and readout circuit, these sensors do not suffer the same drawback of mis-positioning as the skin vibration sensor, but its readout signal still varies with the level of mis-positioning and furthermore different optical properties of skin and tissue, leading to possibly largely-varied level of PD output signal.

Many studies illustrated that the BP can be measured by principle of pulse wave velocity (PWV) (Miyachi et al. 2013). However, the PWV is a challenging calculation since it has many unknown coefficients of artery in

✉ Yung-Hua Kao
yunghwa.kao@gmail.com

¹ Department of Electrical Engineering, National Chiao Tung University, Hsinchu 300, Taiwan

cardiovascular system, and need to consider the different blood flow velocity and blood volume by subjects. Pulse arrival time (PAT) has been proved useful technique to correlation between the BP and PWV (Geddes et al. 1981; Pinheiro et al. 2009). According to early references to discuss, the definition of PAT is from the R-peak of electrocardiogram (ECG) to P-peak of photoplethysmography (PPG) duration (Ding et al. 2016).

Nevertheless, most efforts are employed this time delay method as a surrogate of pulse transit time (PTT) for BP estimation. In fact, the PAT using ECG and finger PPG is similar merely to the known PTT method for estimating BP (Poon and Zhang 2006), where the PAT consists time of PTT and pre-ejection period (PEP). However in recent years, from scientific reports (Martin et al. 2016) and many studies (Yoon et al. 2017) is proposed that PAT may be unreliable for BP measurement. Based on two shortcomings, the first shortcoming, the PAT need to consider the time of PEP in addition to PTT; the second shortcoming, the PTT component represents the time delay between artery to small arteries despite the smooth muscle contraction and relaxation changes that will not responds to BP. In addition, there are also many literatures that use a single PPG sensor to approve the feasibility for calculating the BP (Teng and Zhang 2003; Suzuki and Oguri 2008; Kurylyak et al. 2013; Xing and Sun 2016; Kachuee et al. 2017).

This paper proposes the reflective pulse transit time (R-PTT) as shown in Fig. 1, where the PPI is means interval of percussion wave to next percussion wave. The definition of R-PTT is duration of from percussion wave to dicotic wave. The systolic component of percussion wave ejected from the left ventricle transmitted along a path to the finger. The diastolic component of dicotic wave reflected back from the aorta transmitted to small arteries in lower body which then travels to the finger, therefore the time delay between the percussion wave and dicotic wave is related to R-PTT of pressure waves (He et al. 2014). Capturing the features in reflected wave with PPG signal to calculate BP is very challenge, especially, to designing a

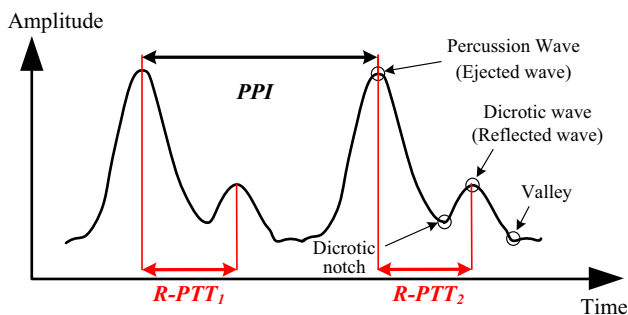


Fig. 1 Typical PPG waveforms with reflected pulse transit times (R-PTT) featured

front-end circuit with high-order filter in case of a limited area and no attenuation by filter. Maximizing the accuracy of BP and minimizing error of R-PTT in this study herein is focused on designing a high-order filter at analog-front-end (AFE) circuit. Since the signal-to-noise (SNR) of raw PPG signal is very low, making the accuracy of BP is serious affected by R-PTT. This influence produces the BP error over the AAMI method 2 is around in tens of milliseconds. To design a high-order filter in AFE circuitry for portable/handheld BP device to measure the R-PTT to calculate the BP is important issue. In this paper, the low-pass (LP) is designed for reducing noise including those due to optical diffraction, electronics and ambient lighting, while the high-pass is for reducing DC drifting caused mainly by breathing and/or subject slow motion.

A new high-order front-end filter for BP monitoring of handheld device has been created in a real-time system. The proposed high order filter is implemented in analog front-end (AFE) circuit. The graphical user interface (GUI) has been developed on the matlab to alarm/record the user status of blood pressure. Following section describes in detail Sects. 2, 3 and 4 in real-time system.

2 Principal of photoplethysmography (PPG) signal

Photoplethysmography (PPG) is known as non-invasive measurement methodology to capture intravascular blood volume change via reflection, absorption and refraction of the lights in varied wavelengths emitted into human skin and tissues below. The associated phenomenon follows the so-called Beer–Lambert Law (Rybynok and Kyriacou

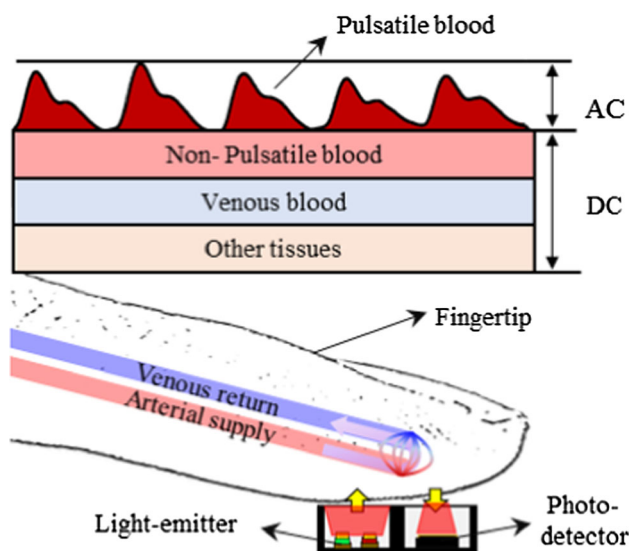


Fig. 2 Principles of PPG measurement fir its reflected type

2010). Figure 2 illustrates the Beer–Lambert Law, where it shows a PPG sensor consisting of LEDs and a PD. The LEDs emits lights in different wavelengths penetrating into skin and tissues. The absorption and refraction of incident lights form generally banana shapes following Lambert–Beer Law (Rybynok and Kyriacou 2010) under the skin and tissue through different blood vessels in varied depths and, finally, some portion of incident lights reaches back to skin surface, detected by the PD. The strength of the PPG signal received by the PD thus depends highly on the attenuation levels through the banana paths, which is also dynamically affected by blood vessel volume changes on the paths, leading to typical detected PPG waveforms as shown in Fig. 2. In this figure, the alternating component (AC) with respect to time is caused by pulsation of arterial vessel volume, while direct component (DC) corresponds to non-pulsatile, baseline arterial vessel volume and others, like skin and tissue.

The incident lights with longer wavelength penetrates deeper into skin/tissue, being able to detect dynamic volume changes of different vessels in varied depths under skin. In this study, the LED at 905 nm is adopted in the PPG sensor to detect dynamical vessel volume changes of arterioles and arteries at different depths.

3 Analog front-end (AFE) circuit

A readout circuitry for a newly-developed handheld BP device has been designed and implemented in proposed real-time system. Figure 3 shows the whole real-time system in block diagram. First of all, the LED is reflected from the fingertip is absorbed by the PD. The wavelength of the

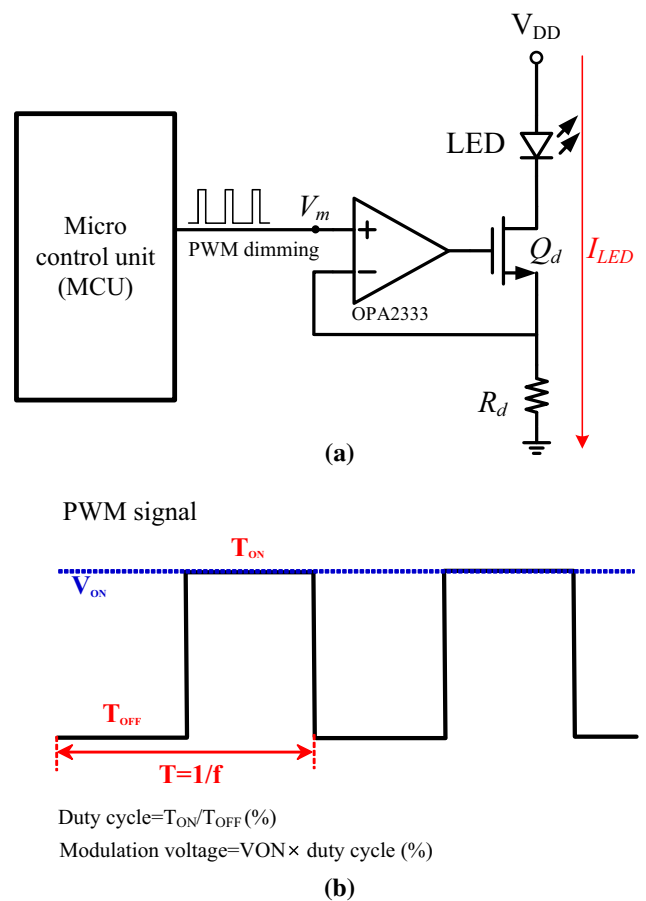


Fig. 4 a LED drive circuit with dimming function, b principle of PWM operation

LED used is 905 nm in infrared. The proposed analog front-end circuit is designed, which includes a led driver, a transimpedance amplifier (TIA), an inverting amplifier, a

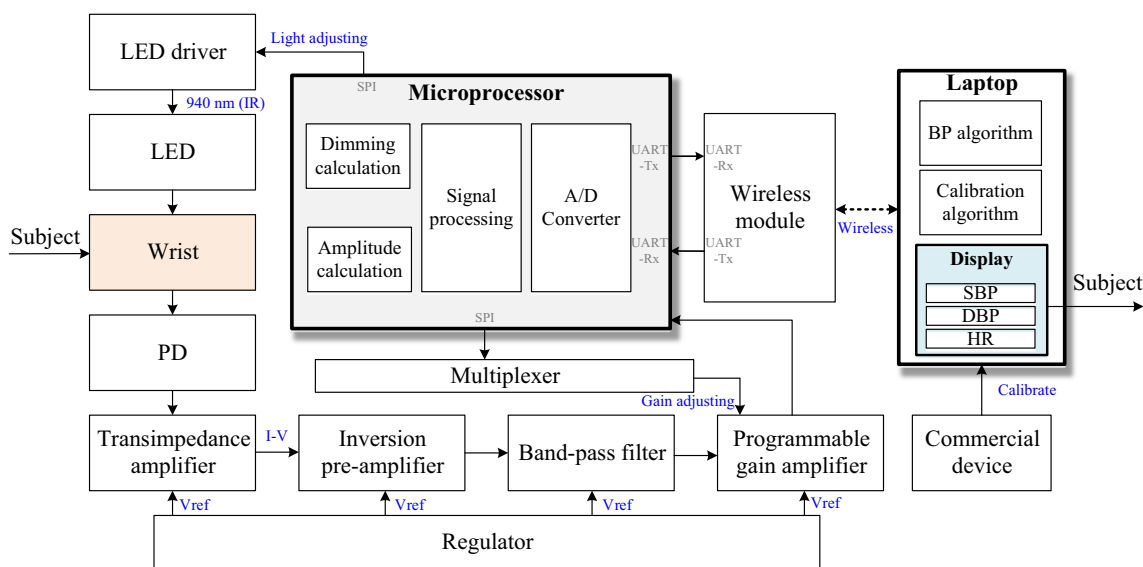


Fig. 3 Functional blocks of system architecture for optical BP measurement

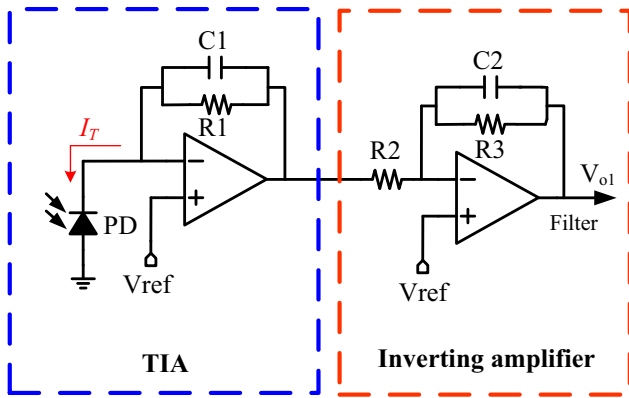
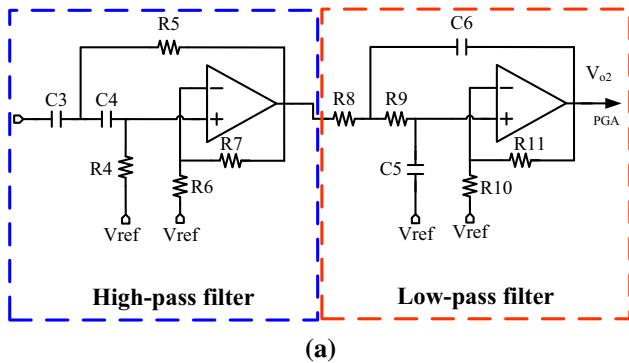
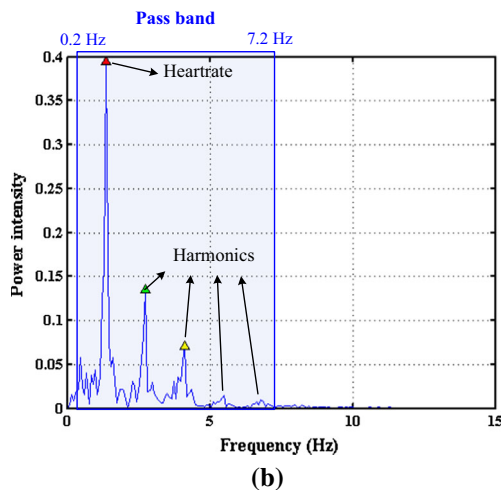


Fig. 5 The low-noise transimpedance amplifier (TIA) and an inverting amplifier

band-pass filter, a programmable gain amplifier (PGA), an analog multiplexer (MUX), low-dropout (LDO) regulator, micro control unit (MCU), which includes an analog-to-digital converter (ADC). Finally, the data is transmitted by a wireless module and then is calculated by the laptop. Note that among all the circuit blocks shown in Fig. 3, special effort by this study has been given to designing a higher-order bandpass filter to maximize the prediction



(a)



(b)

Fig. 6 PPG readout circuit of a 2nd band pass filter; b filtered power spectral density with the entire front-end filters activated

accuracy of BP. The functionalities of each block are elaborated in the followings, including these for the high-order bandpass filter.

3.1 LED driver

Figure 4a shows a schematic diagram of the LED dimming circuit in the optical BP system, which contains an operational amplifier (OPA), a metal oxide semiconductor field effect transistor (MOSFET), a resistor (R_d) and a micro control unit (MCU) to achieve a dimmable LED driver. The tuning of light intensity is based on pulse width modulation (PWM) signal that generated by the MCU as shown in Fig. 4b. The frequency of LED flashing is usually higher than 70 Hz that consider perceivable to the human eye. In this study, the frequency of proposed PWM is designed at 490 Hz by the MCU. During the on-time of pulse width is decided from the requirement of LED current after the digital calculation. Figure 4b shows the principle of the PWM, the duty cycle is equal to T_{ON} divided by T_{OFF} . The requirements of modulating voltage (V_m) is equal to V_{ON} times duty cycle (%), the V_m can be determined based on Eq. (1) as follows,

$$V_m = I_{LED} \times R_d. \tag{1}$$

As shown in Fig. 4b that luminance of LED corresponds to current amplitude through LED itself. The current (I_{LED}) of tunable range designed in this study herein are 3–9 mA.

3.2 Transimpedance amplifier

A current to voltage (I–V) converter proposed in this section herein is optical sensing system that called transimpedance amplifier (TIA) as shown in Fig. 5. The measured PD signal has a current range of approximately 0.5–40 μA that is usually small. The PD response is linear when TIA sample the current, which total current (I_T) consists of a I_{PH} and I_{Dark} , where I_{PH} is the photocurrent and I_{Dark} is the dark current, respectively.

In this study, the TIA is designed for I to V conversion which equipped the resistor (R_1) as 220 K Ohm and capacitor (C_1) as 0.1 μF in first-order filter for reducing the

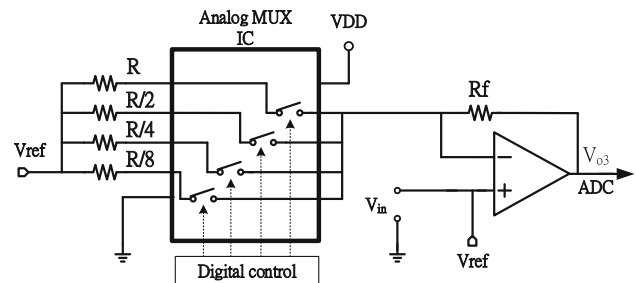


Fig. 7 Programmable gain amplifier



Fig. 8 The BP device with LEDs, PD, readout circuitry and a battery in a PCB and its plastic enclosure

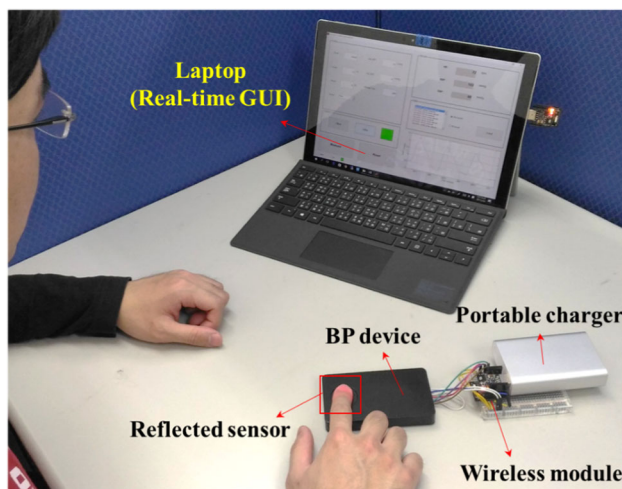


Fig. 9 Experimental system for BP measurement

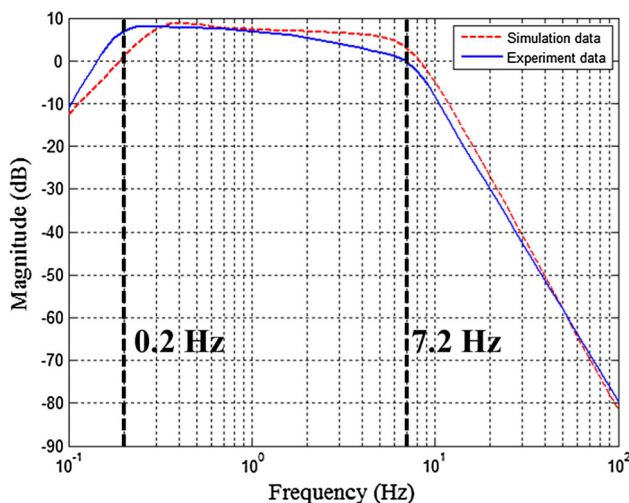


Fig. 10 The experimental frequency responses versus simulated counterparts

shot Noise and thermal noise from the photodiode as detailed in (Okumura et al. 2003). Moreover, the Fig. 5 also shows the de-noisy inverting amplifier in order to invert the TIA output signal, then the R3 and C2 are used for reducing the noise in second-order filter. To this aims, the de-noisy inverting amplifier can keeping the positive output voltage and reducing the noise at the same time.

3.3 High-order band-pass filter

The proposed band-pass filter consists a second-order low-pass (LP) and high-pass (HP) filter as shown in Fig. 6a, in which the HP filter with C3/C4 and R4/R5 are decided as 1 μ F and 680 K, respectively, while the magnified gain is related by R6 and R7. The DC drift of PPG signal is controlled by the HP and V_{ref} , making the PPG signal will oscillated on the V_{ref} level. In addition, the LP filter with R8/R9 and C5/C6 are decided as 210 K and 0.1 μ F, respectively. In this stage, the high-order LP filter is created to reduce the noise in PPG signal, since the BP error is affected from false R-PTT is generated by high noise. By the above paragraph (3.3) the TIA and de-noisy inverting amplifier are also implemented the second-order LP filter in readout circuit, therefore the total order of LP filter designed in this study herein is fourth-order. The cut-off frequency at band-pass filter is designed as 7.2 Hz by the low-pass (LP) band while the high-pass (HP) band is designed as 0.2 Hz. The stop band can be removed the noise and canceled the DC drift from the human movement. This quality of pass band is good for calculating the blood pressure (BP) via the PPG signal. The power spectrum can be seen in Fig. 6b. The stop band can be removed the noise and canceled the DC drift from the human movement. This quality of pass band is good for calculating the blood pressure (BP) via the PPG signal.

3.4 Programmable gain amplifier design

The programmable gain amplifier (PGA) has been established in AFE circuit for controlling the adjusted gain as shown in Fig. 7. Since the measured PPG level for users often varies significantly, the PGA conducts auto gain control (AGC) to tune the signal to full-dynamic range. The MUX is controlled by inner switch via digital circuit to feedback the requirements of the gain for fully-dynamic range.

4 Blood pressure algorithm

The algorithm for calculating blood pressure (BP) is developed herein, which is also set ready for calibration based on a reference device. According to the knows

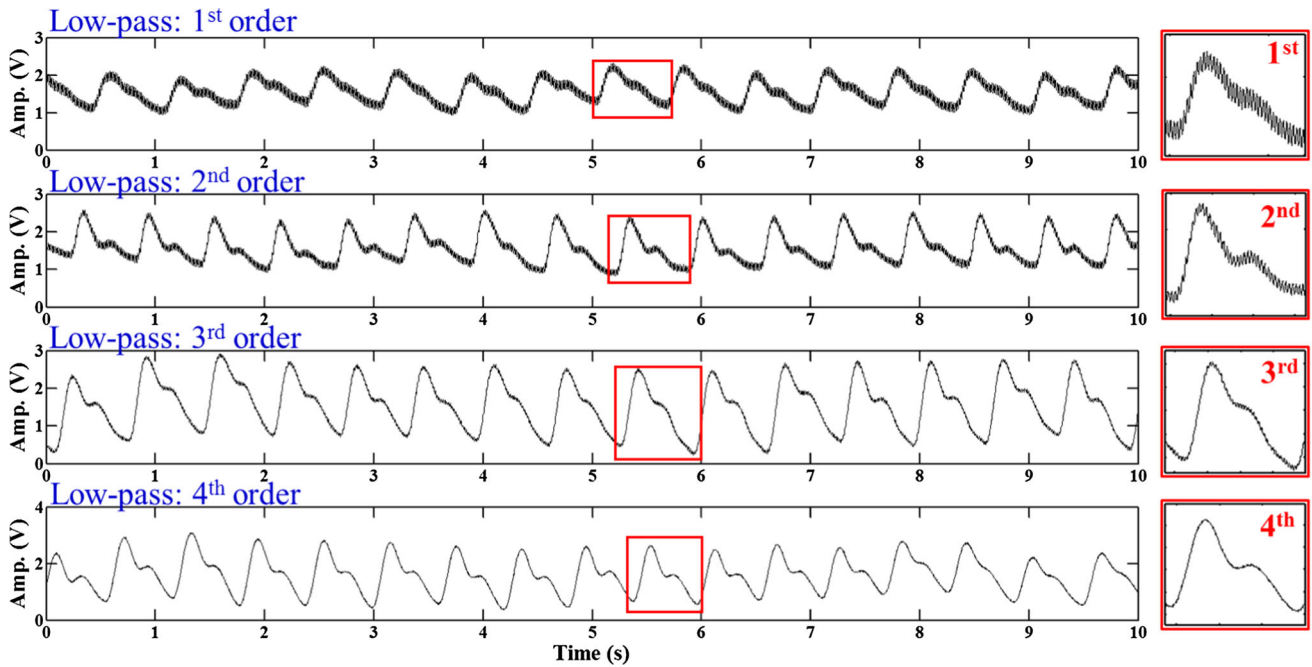


Fig. 11 Filtered PPG waveforms with the filter in orders from first to fourth

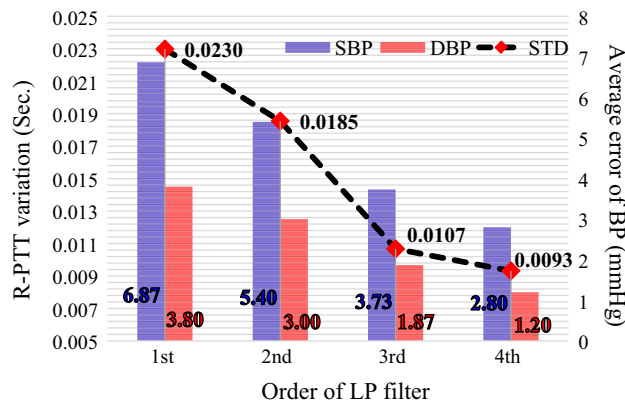


Fig. 12 Standard deviations of measured R-PTTs with different filter orders in 60 sets of cycle data

Moens–Korteweg equation, the *PWV* can be represented in terms of elastic modulus of artery, E_{in} , the thickness of the artery, h , the radius of artery, d , and the density of blood, ρ , by the, i.e.,

$$PWV = \sqrt{\frac{E_{in}h}{2\rho d}}, \tag{2}$$

which the E_{in} is exponentially correlated BP by (Hughes et al. 1979),

$$E_{in} = E_0 e^{\alpha P}, \tag{3}$$

where E_0 is without pressure of elastic modulus, α is a coefficient relating to human vessel and P is the mean of

blood pressure (*MBP*) which is substitute (3) can be expressed,

$$MBP = K_b + \frac{2}{\alpha} \ln\left(\frac{L}{R - PTT}\right)^2, \tag{4}$$

where K_b is a calibrated parameter for depending on the subject, L is a local distance along the aorta from measured point to lower body, $R-PTT$ is the reflected pulse transit time, which is the time of single wave reflection from lower body to measured point, as shown in Fig. 2 definition. The *MBP* is estimated known as $1/3 \cdot SBP + 2/3 \cdot DBP$, where the *SBP* is systolic blood pressure while *DBP* is diastolic blood pressure. Based on Eq. (4) that can be derivation,

$$DBP = -\frac{1}{3} \left(\frac{K_a \cdot L^2}{R - PTT^2} \right) + K_b + \frac{2}{\alpha} \ln\left(\frac{L}{R - PTT}\right)^2, \tag{5}$$

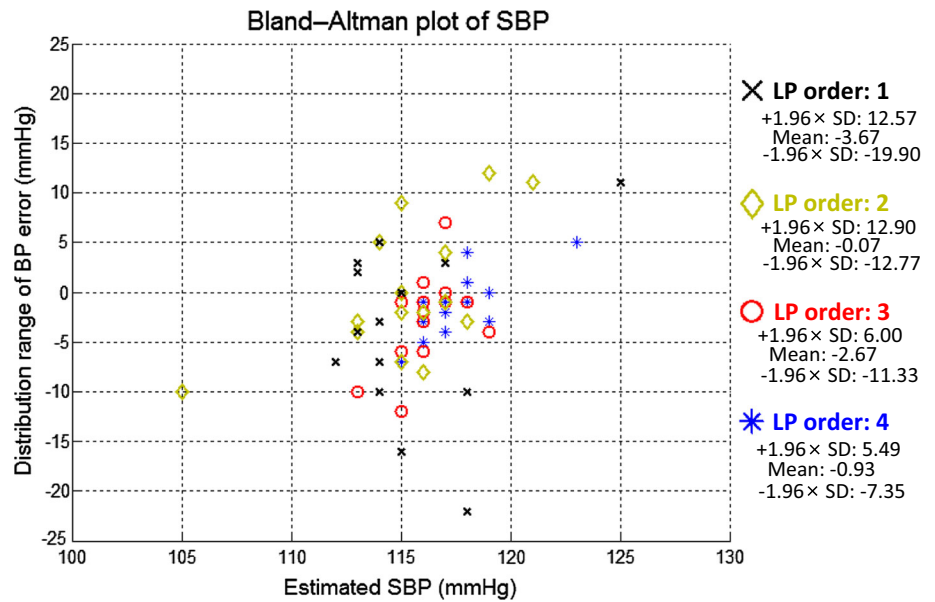
where K_a is the calibrated parameter for depending on the subject.

On the other hand, based on the known Bramwell–Hill equation (Bramwell and Hill 1922), the BP can be calculated by the known pulse wave velocity (*PWV*). In this study, local *PWV* is the distance traveled L divided by time $R-PTT$, which is equivalent of the reflected wave,

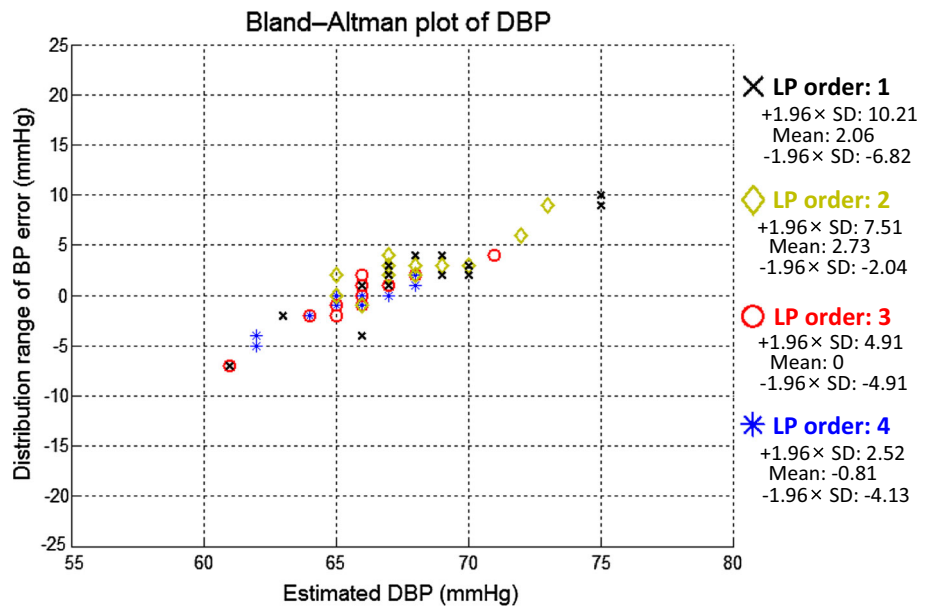
$$PWV = \sqrt{\frac{V}{\rho(dV/dP)}} = \frac{L}{R - PTT}, \tag{6}$$

where the ρ is blood density, V is the blood volume in

Fig. 13 Distribution range of measured BP error by different filter order in 60 sets of data at **a** SBP; **b** DBP



(a)



(b)

artery and dP is the blood pressure difference between SBP and DBP that can indicated,

$$dP = SBP - DBP, \tag{7}$$

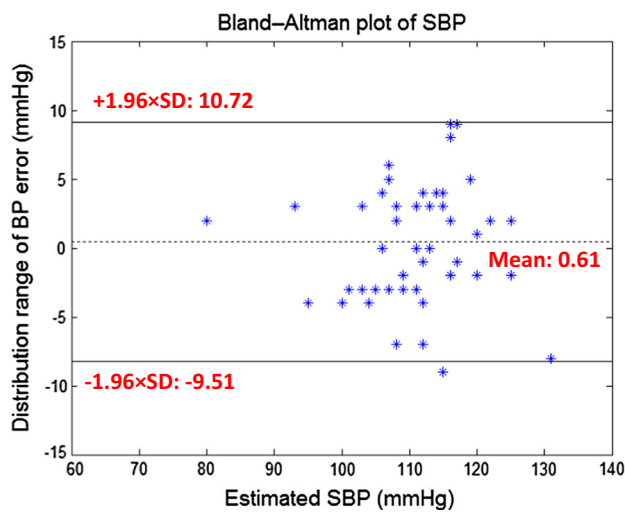
substituting of Eq. (7) into Eq. (6), the systolic can be represented,

$$SBP - DBP = \frac{\rho \cdot dV}{V} \left(\frac{L}{R - PTT} \right)^2, \tag{8}$$

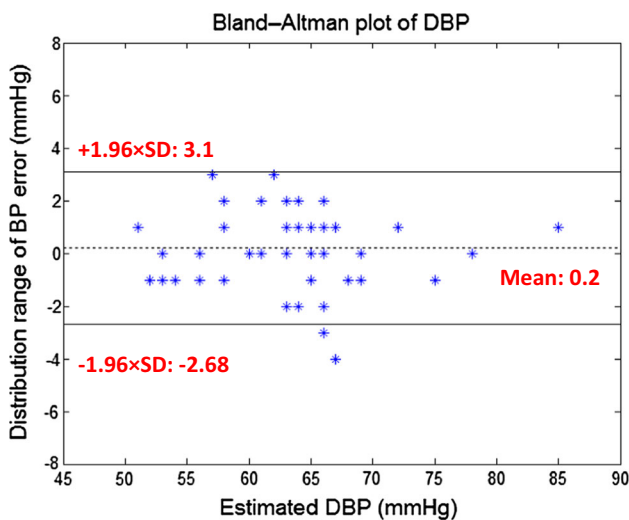
where the dV is the blood volume changes in artery. Based on the derivation of Eq. (8) can be expressed,

$$SBP = DBP + K_a \cdot \left(\frac{L}{R - PTT} \right)^2. \tag{9}$$

The calibration parameters (K_a , K_b , L) are obtained by subject for one times calibration. Using the gold standard of reference device to calibrate Eqs. (5) and (8), then the proposed BP device can measured the R - PTT to calculate the SBP and DBP (Kao et al. 2016).



(a)

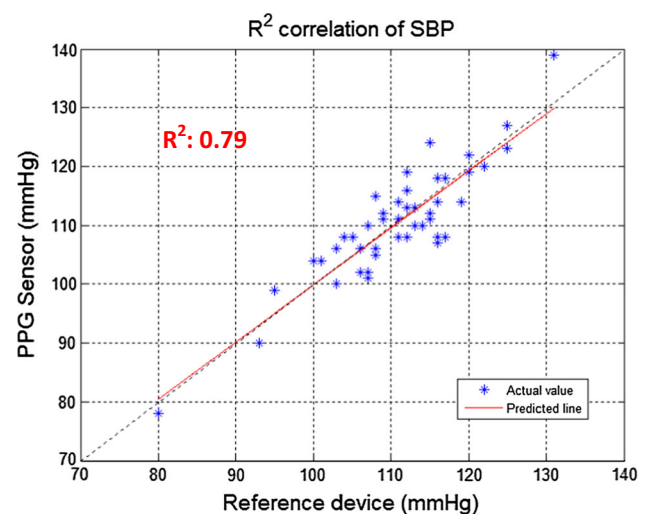


(b)

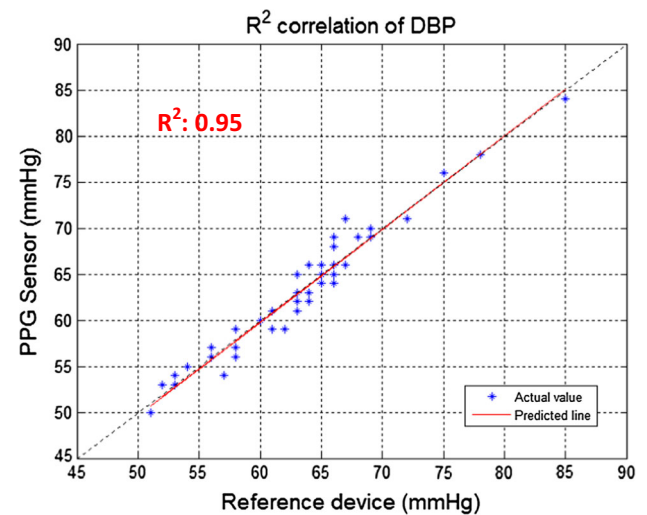
Fig. 14 Distribution range of measured BP error by 46 subject data at **a** SBP; **b** DBP

5 Experimental results

A high-order front-end filter is developed in real-time system for maximizing the BP accuracy. The photo of sensor and circuit configuration is designed in BP device as shown in Fig. 8, which the sensor is reflected type on LED/PD module while the wavelength of LED is selected as 905 nm. The circuit configuration includes the LED driver, TIA, 4th-order filter, PGA, LDO and the battery as also shown in Fig. 8. The photo of experimental set up as shown in Fig. 9. A GUI is created by the Matlab, which has a personal information, a calibration function, a display of continuous BP measurements, and an indicator of signal quality.



(a)



(b)

Fig. 15 Correlation plot of BP by 46 subject data at **a** SBP; **b** DBP

The estimation BP results are successfully conducted in this experiment. The experimental results is validated from commercial BP monitoring as HEM-7310. The experimental can be divided into two steps, first-step is maximizing the accuracy of BP with different filter-order in one subject, while the second-step is maximizing the accuracy of BP with fourth-order in 46 subject. Firstly, the high-order filter is validated from different PPG signal, since the R-PTT/BP is affected from high-noisy PPG signal. Designing a high-order filter to minimize R-PTT/BP error is a major goal in this study. Figure 10 shows the experimental frequency responses versus simulated counterparts. It is clearly seen from this figure that the expected performance based on design matches closely the experimental counterparts. Figure 11 shows the results with filter of varying degrees in PPG signal, which represents the

first-order to fourth-order filter from top to bottom, respectively. As different results can be found the characteristics (i.e., percussion wave, reflected wave, dicrotic notch and valley) of PPG signal is caused by noise. Figure 12 shows the standard deviation (SD) of R-PTT variation corresponding to different filter order, which is also corresponding to average error of BP. As mentioned, the 60 data is measured by 15 trial in each filter at the same subject for verifying the performance of high-order filter. The standard deviation of R-PTT variation are calculated as 0.023, 0.0185, 0.0107 and 0.0093 (ms) in filter of first-order to fourth-order, respectively. On the other hand, the average error of BP as 6.87/3.80, 5.40/3.00, 3.73/1.87 and 2.80/1.20 (mmHg) at SBP/DBP, respectively. The R-PTT method has a challenge for capturing the time interval from percussion wave to reflected wave. Since taking the features of reflected wave is easily affected by electronic noise or ambient light noise. Therefore, designing a high-order filter is important for BP measurement in this system. Based on the experimental results, the high-order filter can reduce most of noise that is used for increasing the R-PTT accuracy, especially after the fourth-order filter can see the STD in convergence results. The results of R-PTT variation is based on the measured first-order to fourth-order filter, which the STD at first-order filter is 0.023 (ms), while the better fourth-order filter is 0.0093 (ms). The variation rate of R-PTT is effectively reduced by 40%.

Figure 13a, b shows the Bland–Altman plot of SBP and DBP at the same subject for 60 trial experiment, the x -axis represents the range of BP estimation (unit: mmHg), while the y -axis represents the distribution range of BP error (unit: mmHg) with different filter order. The black-cross indicates first-order LP filter; the khaki-diamond indicates second-order LP filter; the red-circle indicates third-order LP filter; and the blue-asterisk indicates fourth-order LP filter. The SBP of 95% confidence intervals and mean in first-order to fourth-order filter can represents, -19.90 to 12.57 , mean as -3.67 ; -12.77 to 12.90 , mean as -0.07 ; -11.33 to 6.00 , mean as -2.67 ; -7.35 to 5.49 , mean as -0.93 , respectively. The DBP of 95% confidence intervals and mean in first-order to fourth-order filter can represents, -6.82 to 10.21 , mean as 2.06 ; -2.04 to 7.51 , mean as 2.73 ; -4.91 to 4.91 , mean as 0 ; -4.13 to 2.52 , mean as -0.81 , respectively. Figure 14a, b shows the Bland–Altman plot of SBP and DBP using the fourth-order filter to conduct the experiment for 46 subject. The 95% confidence interval and mean are drawing in black solid-lines and dot-line, respectively, which the SBP is -9.51 to 10.72 and mean as 0.61 , the DBP is -2.68 to 3.1 and mean as 0.2 . It was observed the most of points were within the 95% confidence limits. For the R^2 correlation is estimated by Fig. 15a, b, which the correlation of SBP and DBP are 0.79 and 0.95 respectively, which are the better than most of

prior arts (Gao et al. 2016; Shin and Min 2017; Miao et al. 2017).

6 Conclusion

Towards maximizing the BP accuracy is validated by the high-order filter via the optical BP sensor. The proposed BP algorithm utilizes the R-PTT for calculating the SBP and DBP. The STD of R-PTT is corresponding to the SBP/DBP when STD variation is increasing then the average error of SBP/DBP is also increasing. Summary, the lowest SBP/DBP error are 2.8/1.2 mmHg at fourth-order filter in same subject with 60 data. The high-order filter is proved for equipping in the BP system. As for the final results, the participants of 46 subjects are includes 38 males and 8 females, the ages are approximately 23–35. Based on the Bramwell–Hill and Moens–Korteweg equation to derivation the SBP and DBP with HEM-7310 calibration. The research develops an accurate estimate on BPs by the continuous BP device. The BP estimation accuracy of the algorithm is evaluated using the British Hypertension Society (BHS) (O’Brien et al. 1990) and Association for the Advancement of Medical Instrumentation (AAMI) standards (AAMI 2002). Based on the BHS and AAMI, the SBP and DBP is approved as grade B and A, respectively, and also validated by AAMI II criterion in (IEEE Standards 2014).

Acknowledgement This work was supported in part by the Novel Bioengineering and Technological Approaches to Solve Two Major Health Problems in Taiwan sponsored by the Taiwan Ministry of Science and Technology Academic Excellence Program under Grant Number: MOST 106-2633-B-009-001 and 107-2633-B-009-003. The authors appreciate the supports from MOST 106-2221-E-009 -089, 106-2218-E-009 -011 and Chunwha Prcture Tubes, Ltd.

References

- Ahmad S, Bolic M, Dajani H, Groza V, Batkin I, Rajan S (2010a) Measurement of heart rate variability using an oscillometric blood pressure monitor. *IEEE Trans Instrum Meas* 59(10):2575–2590
- Ahmad S, Chen S, Souerdan K, Batkin I, Bolic M, Dajani H et al. (2010b) A prototype of an integrated blood pressure and electrocardiogram device for multi-parameter physiologic monitoring. In: *Proceedings of IEEE conference on instrumentation measurement technology*, pp 1244–1249
- American National Standard for Electronic or Automated Sphygmomanometers, ANSI/AAMI SP 10 2002, Association for the Advancement Instrumentation, Arlington, 2002
- Bramwell JC, Hill AV (1922) The velocity of the pulse wave in man. *Proc R Soc Lond B* 93(652):298–306
- Ding XR, Zhang YT, Liu J, Dai WX, Tsang HK (2016) Continuous cuffless blood pressure estimation using pulse transit time and photoplethysmogram intensity ratio. *IEEE Trans Biomed Eng* 63(5):964–972

- Dupuis P, Eugene C (2000) Combined detection of respiratory and cardiac rhythm disorders by high-resolution differential cuff pressure measurement. *IEEE Trans Instrum Meas* 49(3):498–502
- Gao M, Olivier NB, Mukkamala R (2016) Comparison of noninvasive pulse transit time estimates as markers of blood pressure using invasive pulse transit time measurements as a reference. *Physiol Rep*. <https://doi.org/10.14814/phy2.12768>
- Geddes LA, Voelz MH, Babbs CF, Bourland JD, Tacker WA (1981) Pulse transit time as an indicator of arterial blood pressure. *Psychophysiology* 18:71–74
- He X, Goubran RA, Liu XP (2014) Secondary peak detection of PPG signal for continuous cuffless arterial blood pressure measurement. *IEEE Trans Instrum Meas* 63(6):1431–1439
- Huang F, Lin K, Gao F, Chen C, Shao H, Wang B (2015) A 1.2-V 7.2- μ w ECG AFE with continuous time self-calibration filters. In: *IEEE 11th international conference on ASIC (ASICON)*, pp 1–4
- Hughes DJ, Babbs CF, Geddes LA, Bourland JD (1979) Measurements of Young's modulus of elasticity of the canine aorta with ultrasound. *Ultrason Imaging* 1(4):356–367
- IEEE Standards Association (2014) IEEE standard for wearable cuffless blood pressure measuring devices. *IEEE Standard* 1708–2014, pp 1–38
- Kachuee M, Kiani MM, Mohammadzade H, Shabany M (2017) Cuffless blood pressure estimation algorithms for continuous health-care monitoring. *IEEE Trans Biomed Eng* 64(4):859–869
- Kaniusas E, Pflutzner H, Mehnert L, Kosel J, Tellez-Blanco C, Varoneckas G, Alonderis A, Meydan T, Vazquez M, Rohn M, Merlo AM, Marquardt B (2006) Method for continuous non-disturbing monitoring of blood pressure by magnetoelastic skin curvature sensor and ECG. *IEEE Sens J* 6(3):819–828
- Kao YH, Tu TY, Chao PCP, Lee YP, Wey CL (2016) Optimizing a new cuffless blood pressure sensor via a solid-fluid-electric finite element modelling with consideration of varied mis-positionings. *J Microsyst Technol* 22:1437–1447
- Kurylyak Y, Lamonaca F, Grimaldi D (2013) A Neural Network-based method for continuous blood pressure estimation from a PPG signal. In: *International conference of the IEEE in instrumentation and measurement technology*, pp 280–283
- Lee SY, Cheng CJ (2009) Systematic design and modeling of a OTA-C filter for portable ECG detection. *IEEE Trans Biomed Circuits Syst* 3(1):53–64
- Lin WQ, Wu HH, Su CS, Yang JT, Xiao JR, Cai YP, Chen GZ (2017) Comparison of continuous noninvasive blood pressure monitoring by TL-300 with standard invasive blood pressure measurement in patients undergoing elective neurosurgery. *J Neurosurg Anesthesiol* 29(1):1–7
- Mahmoud SA, Bamakhrumah A, Al-Tunaiji SA (2014) Six order cascaded power line notch filter for ECG detection systems with noise shaping. *Circuits Syst Signal Process* 33(8):2385–2400
- Martin SLO, Carek AM, Kim CS, Ashouri H, Inan OT, Hahn JO, Mukkamala R (2016) Weighing scale-based pulse transit time is a superior marker of blood pressure than conventional pulse arrival time. *Sci Rep* 6:39273
- Miao F, Fu N, Zhang YT, Ding XR, Hong X, He Q, Li Y (2017) A novel continuous blood pressure estimation approach based on data mining techniques. *IEEE J Biomed Health Inform* 21(6):1730–1740
- Miyauchi Y, Koyama S, Ishizawa H (2013) Basic experiment of blood pressure measurement which uses FBG sensors. In: *Proceedings of IEEE international conference instrumentation measurement*, pp 1767–1770
- O'Brien E, Petrie J, Littler W, de Swiet M, Padfield PL, O'malley K, Atkins N (1990) The British Hypertension Society protocol for the evaluation of automated and semi-automated blood pressure measuring devices with special reference to ambulatory systems. *J Hypertens* 8:607–619
- Okumura M, Tanimoto H, Itakura T, Sugawara T (1993) Numerical noise analysis for nonlinear circuits with a periodic large signal excitation including cyclostationary noise sources. *IEEE Trans Circuits Syst I: Fundam Theory and Appl* 40(9):581–590
- Pinheiro E, Postolache O, Girao P (2009) Pulse arrival time and ballistocardiogram application to blood pressure variability estimation. In: *Proceedings of the IEEE international workshop on medical measurement and applications*, pp 132–136
- Poon C, Zhang Y (2006) Cuff-less and noninvasive measurements of arterial blood pressure by pulse transit time. In: *2005 IEEE engineering in medicine and biology 27th annual conference*, pp 5877–5880
- Rybynok VO, Kyriacou PA (2010) Beer-lambert law along non-linear mean light pathways for the rational analysis of photoplethysmography. *J Phys Conf Ser* 238(1):012061
- Sharma M, Barbosa K, Ho V, Griggs D, Ghirmai T, Krishnan SK, Cao H (2017) Cuff-less and continuous blood pressure monitoring: a methodological review. *Technologies* 5(2):21
- Shin H, Min SD (2017) Feasibility study for the non-invasive blood pressure estimation based on ppg morphology: normotensive subject study. *Biomed Eng Online* 16(1):10
- Silvani A, Grimaldi D, Vandi S, Barletta G, Vetruigno R, Provini F et al (2008) Sleep-dependent changes in the coupling between heart period and blood pressure in human subjects. *Am J Physiol Regul Integr Comp Physiol* 294:1686–1692
- Suzuki S, Oguri K (2008) Cuffless and non-invasive systolic blood pressure estimation for aged class by using a photoplethysmograph. In: *Proceedings of the 30th annual international conference of the IEEE in engineering in medicine and biology society*, pp 1327–1330
- Teng XF, Zhang YT (2003) Continuous and noninvasive estimation of arterial blood pressure using a photoplethysmographic approach. In: *Proceedings of the 25th annual international conference of the IEEE in engineering in medicine and biology society*, vol 4, pp 3153–3156
- Tu TY, Chao PCP, Lee YP (2013) A new non-invasive cuff-less blood pressure sensor. In: *2013 IEEE Sensors in Baltimore, MD*, pp 1–4
- Tu TY, Kao YH, Chao PC, Lee YP (2014) Optimizing a new blood pressure sensor for maximum performance based on finite element model. In: *Conference on IEEE sensors, Valencia, Spain*, pp 1873–1876
- WHO (2015a) Cardiovascular diseases (CVDs). WHO, Geneva
- WHO (2015b) World health statistic 2015. World Health Organization, Geneva
- Xing X, Sun M (2016) Optical blood pressure estimation with photoplethysmography and FFT-based neural networks. *Biomed Opt Express* 7(8):3007–3020
- Yoon YZ, Kang JM, Kwon Y, Park S, Noh S, Kim Y, Park J, Hwang SW (2017) Cuff-less blood pressure estimation using pulse waveform analysis and pulse arrival time. *IEEE J Biomed Health Inform* PP(99):1